Desalination and Water Treatment
www.deswater.com
doi: 10.5004/dwt.2023.29769

302 (2023) 147–154
August

Preparation of Pd/MnO_2 catalyst and its catalytic hydrogenation reduction of Cr(VI)

Yuhong Cao, Dianzhao Li*, Dailiang Yu, Fan Wen

School of Ecology and Environment, Anhui Normal University, Wuhu, China 241002, emails: 1917469869@qq.com (D. Li), hong923@ahnu.edu.cn (Y. Cao), 1052877996@qq.com (D. Yu), 1543520826@qq.com (F. Wen)

Received 2 April 2023; Accepted 13 July 2023

ABSTRACT

Liquid catalytic hydrogenation is a green, economical and non-polluting technology that can effectively reduce and remove pollutants from water. In this study, Pd/MnO_2 catalyst was synthesized with precious metal Pd as the active component and MnO_2 as the carrier, and formic acid was used as the hydrogen source for liquid catalytic hydrogenation to reduce Cr(VI); And the composition and morphology of Pd/MnO_2 catalyst were characterized by X-ray diffraction, transmission electron microscopy and scanning electron microscopy; in the reaction of Cr(VI) reduction, the effects of different catalysts, catalyst dosage, initial concentration of Cr(VI), pH and different Pd loadings on the reduction of Cr(VI) were investigated. The results of the experimental tests showed that the reduction of Cr(VI) by Pd/MnO_2 was 93.2%, the reduction of Cr(VI) by MnO_2 was 20.9%, and the reduction of Cr(VI) by MnO_2 after loading Pd was 4.46 times higher than that by unloaded Pd. The results of the study showed that the reduction of Cr(VI) by Pd/MnO_2 was not significant when the pH was 2, the initial concentration of Cr(VI) was 1 mM, the loading of Pd was 0.74 wt.%, and the catalyst dosage was 0.25 g/L, the Pd/MnO_2 catalyst could reduce Cr(VI) in water more rapidly and effectively; the Pd/MnO_2 catalyst is a new type of rapid and efficient catalyst for Cr(VI) reduction.

Keywords: Cr(VI); Catalytic hydrogenation; Pd/MnO_2; Load

1. Introduction

Although microplastics (MPs) and sulfonamides (SAs) are emerging aquatic pollutants [1], but the Cr pollution in water still can't be ignored. In the aquatic ecological environment, Cr is dominated by hexavalent chromium (Cr(VI)) and trivalent chromium (Cr(III)) [2]. Even for the same chromium element, these two valent chromium ions have opposite physicochemical properties. Cr(III) is mainly presented in the form of cation, while Cr(VI) usually exists in the form of anion, because the chromium environment pH is different, so the form of chromium is also different, the commonalities are CrO_4^{2-}, Cr_2O^{2-}, $HCrO_4^-$. A visual simulation of the form of Cr(VI) and Cr(III) presence in the H_2O system was performed by Kocaoba and Akcin [3]. In nature, Cr(VI) affects the rooting of plants, the reproduction of organisms in the soil, and the respiratory system of marine organisms. Cr(VI) is a highly toxic substance that causes human cancer, which is mutagenic and can cause many health problems [4]. Cr(VI) is very mobile. Once entering the human body, it is easy to grow together and damage human organs, such as liver and kidney injury, lung cancer, skin inflammation, gastrointestinal damage and other problems. The Environmental Protection Agency (USEPA) has consistently included Cr(VI) on the list of toxic pollutants and set the maximum allowable concentration allowed in drinking water at 50 μg/L [5].

* Corresponding author.

In the past, many researchers have been trying to promote effective chromium removal and treatment techniques, and they have established a variety of techniques to control chromium pollution from the physical, chemical and biological perspectives. These technologies are mainly divided into three categories: physical and chemical technology, electrochemical technology, advanced oxidation technology, and biological treatment method [6–13]. Although these methods have certain advantages, most of them involve high energy consumption, high cost of treatment, low efficiency, complex implementation steps as well as secondary pollution and other problems. Catalytic hydrogenation technology has the characteristics of simple device, convenient operation, low energy consumption, high efficiency and no secondary pollution. The reaction can be carried out at room temperature and pressure, usually with hydrogen as the reducing agent and precious metal as the active component [14]. The system includes four parts: reactant, solvent, hydrogen source and catalyst. The pollutants that can be treated in liquid-phase catalytic hydrogenation reduction technology are usually inorganic salt ions with high-priced state and strong oxidation properties, such as BrO^{3-}, NO^{3-}, Cr(VI) and Cu(II) [15–18]. Compared with other precious metals, the precious metal Pd has a relatively strong ability to activate hydrogen, and is widely used as an active component [19]. Manganese dioxide has a strong oxidation properties and adsorption capacity [20], mineral-rich [21,22], acid corrosion resistance [21], low toxicity [23], narrow band gap, low production cost, high compatibility with environmental advantages. These advantages make manganese dioxide become a promising and widely used material [24]. In environmental purification systems, manganese dioxide can be used as an adsorbent material for the removal of heavy metals, dyes and microwave contamination, as well as a thermal catalyst, photocatalyst and a catalyst for the degradation of pollutants (water and gas, organic and inorganic pollutants). In this paper, MnO_2 is used as the carrier, and the Pd particles are evenly distributed on the surface of MnO_2, which avoids the agglomeration of Pd particles and increases the contact surface between the active component Pd and formic acid solution, which will make formic acid produce more active hydrogen and hydrogen gas and make the reduction of Cr(VI) faster. Compared with H_2, formic acid is a relatively safe, highly efficient, convenient hydrogen storage and transportation material, and it is more widely used [25,26].

In this study, Pd/MnO_2 was synthesized by impregnation and applied to the catalytic hydrogenation and reduction of Cr(VI). It not only improves the reduction rate of MnO_2 to Cr(VI), but also can reuse the manganese dioxide, saving the economic cost of governance, and satisfying the requirements of green chemistry.

2. Material and methods

2.1. Materials

MnO_2, $PdCl_2$ and ascorbic acid were purchased from Shanghai Maclean Biochemical Technology Co., (China). The starch was purchased from Sinopharm Chemical Reagent Co., Ltd., (China) and sodium hydroxide from Xilong Chemical Co., Ltd., (China) pure water.

2.2. Catalyst preparation

Synthesis of catalyst Pd/MnO_2: add starch solution to the sample tube, add $PdCl_2$ solution to it, mix, mix the solution neutral with NaOH solution, add MnO_2 material to it, ultrasonic mix, and then transfer to a beaker. Add an appropriate amount of ascorbic acid to another beaker, then add distilled water and an appropriate amount of starch solution, respectively, and mix well. The ascorbic acid solution was added to one droplet and one dispersed solution of MnO_2 and $PdCl_2$ at room temperature and continued for 1 h. The Pd/MnO_2 composite was obtained by centrifugation, washing and vacuum drying.

2.3. Catalyst characterization

X-ray diffraction Bruker D8 Advance, Germany, the body phase composition, microstructure and crystal type of matter are analyzed qualitatively. The catalyst was carefully pressed into a smooth glass slide groove and put into the powder diffractor to test. The powder diffraction instrument has an operating voltage of 40 kV, an operating current of 40 mA, a 2θ range of 10°–80° for high/wide angle scanning, a scanning speed of 5°/min, and a scanning step length of 0.02°/step.

Transmission electron microscope American FEI Talos F200X G2, take some samples dispersed into the ethanol solution for ultrasound, and then take a few drops of dispersed liquid added on the copper network, after drying, with the model of American FEI Talos F200X G2, acceleration voltage of 200 kV, energy spectrum model EDS super-X, photo morphology.

2.3.1. Scanning electron microscopy

Test reference step: take trace samples directly adhered to the conductive adhesive, and use Oxford Ultim Max 65 sputtering coating instrument for 45 s, 10 mA. Then use Hitachi Regulus8100 scanning electron microscope to take the sample morphology, energy spectrum mapping, the acceleration voltage is 3 kV, the acceleration voltage is 20 kV, and the detector is SE2 secondary electron detector.

2.3.2. X-ray photoelectron spectroscopy

The elemental composition and valence distribution of the material surface were analyzed and determined using a Scientific K-Alpha electron spectrometer manufactured by Thermo, USA. The instrument was equipped with Al K-rays as the excitation source (hv = 1,486.6 eV) to analyze the elemental energy spectrum at the atomic scale and depth of the material surface.

2.4. Liquid-phase catalytic hydrogenation for the reduction of Cr(VI)

First take 50 mL colorimetric tubes, take 0.1 mol/L potassium dichromate reserve solution, prepare the concentration of 0, 0.25, 0.5, 0.75 and 1 mmol/L solution, then take pure water as the reference solution, the standard solution concentration (mmol/L) as the abscissa, absorbance (Abs) as the

ordinate, and finally the standard curve of the solution measured at the maximum absorption wavelength of 540 nm is $y = 64.63x$, $R^2 = 0.9997$. The catalytic hydrogenation reduction reaction of Cr(VI) was conducted in a 250 mL tapered bottle to prepare 200 mL of Cr(VI) aqueous solution. The catalyst was magnetically stirred for 0.5 h. The reaction pH was set to 2 with excessive formic acid and 1 mol/L of NaOH. All samples were filtered using 0.45 μm drainage filter, and the absorbance of Cr(VI) was detected by a UV spectrophotometer. The detection wavelength was 540 nm, and the actual concentration was calculated from the standard curve of the pollutants measured by the UV spectrophotometer.

3. Results and discussion

3.1. Catalyst characterization

3.1.1. Radioactive diffraction (XRD)

Fig. 1 shows the X-ray diffraction (XRD) map of MnO_2 and Pd/MnO_2. As can be seen from the following figure, the characteristic diffraction peaks of MnO_2 are 26.5, 37.4, 59.4 and 72.2. The manganese dioxide carrying palladium showed new characteristic diffraction peaks at 28.5, 42.5 and 67.4. Compared with the standard map, these two peaks are the diffraction peaks of palladium. The appearance of the palladium characteristic peak indicates that the loaded palladium particles exist on the surface of the catalyst and have a cubic crystal structure. It shows that the Pd particles were successfully loaded onto the carrier MnO_2; moreover, the loading process of Pd did not change the structure of the carrier.

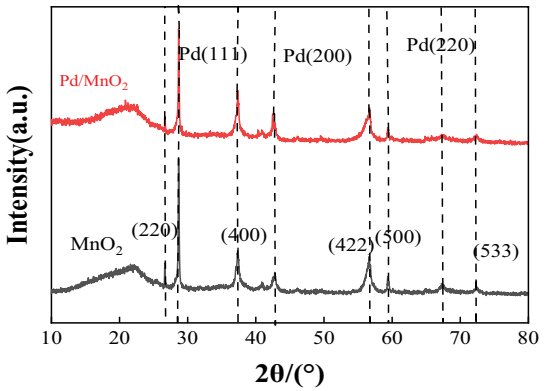

Fig. 1. X-ray diffraction profile of the catalyst.

3.1.2. Transmission electron microscopy

The transmission electron microscopy (TEM) diagram of Pd/MnO_2 clearly shows the morphology of the carrier manganese dioxide and the precious metal palladium. The load of palladium particles on the surface of the catalyst is relatively uniform. According to the particle size of palladium particles on the lens map. In Fig. 2b, the distribution of palladium particles on Pd(0.74)/MnO_2 ranges from 2–16 nm.

3.1.3. Scanning electron microscopy

It can be seen from Fig. 3 that the size of MnO_2 nanomaterials is about 200–300 nm, and the flower shape of MnO_2 in Pd/MnO_2 composites is laminar, and it can be clearly seen that Pd nanoparticles are distributed on MnO_2, indicating that the Pd has been successfully loaded on the surface of MnO_2.

3.1.4. X-ray photoelectron spectroscopy

The surface composition of the catalyst Pd/MnO_2 was obtained by X-ray photoelectron spectroscopy (XPS) analysis. For Pd/MnO_2, Pd has two highly asymmetric peaks in the 3d region, which indicates that the peaks of Pd are compounded by multiple peaks, representing different Pd species on the catalyst. In this study, the XPS curves were fitted to split peaks in order to quantify the content of each species: Pd on Pd/MnO_2 consists mainly of metallic Pd (Pd^0) and cationized Pd (Pd^{n+}). The presence of Pd^{n+} is mainly due to the strong interaction of Pd with the oxygen-containing functional groups on the surface of MnO_2 to transfer electrons from the Pd surface to MnO_2 (Fig. 4).

3.2. Effect of different conditions on the catalytic hydrogenation reduction of Cr(VI)

3.2.1. Blank experiment

To verify that the reduction of Cr(VI) is a chemically catalyzed reaction, a series of blank experiments were carried

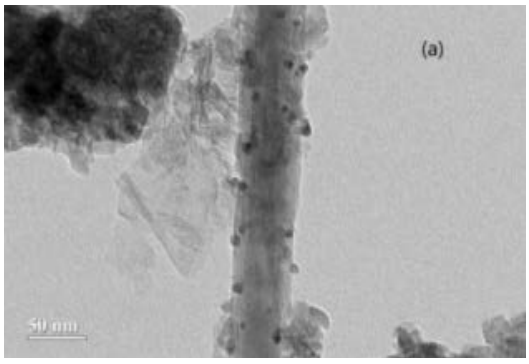

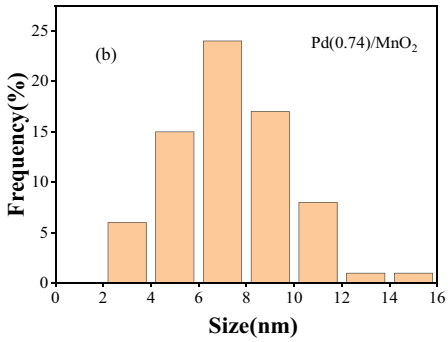

Fig. 2. Transmission electron microscopy images and histograms of Pd particle-size distributions of the supported catalysts.

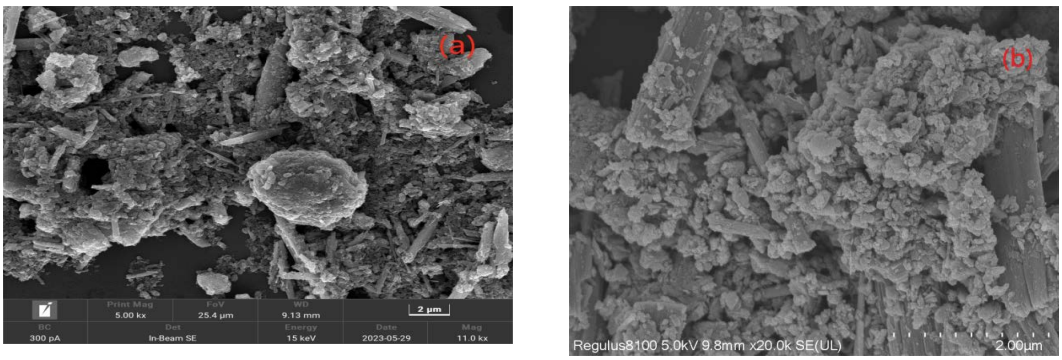

Fig. 3. Scanning electron microscopy patterns of (a) MnO_2 and (b) Pd/MnO_2.

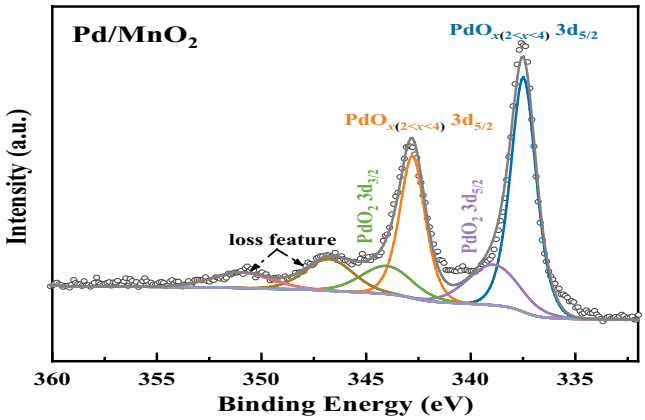

Fig. 4. X-ray photoelectron spectra of Pd/MnO_2 catalysts.

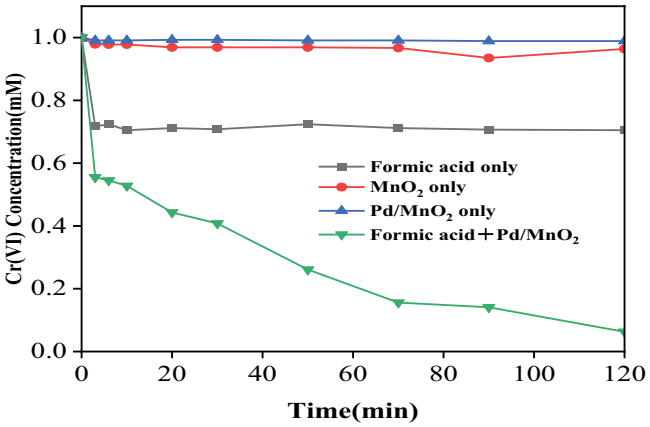

Fig. 5. Blank experiment.

out. The samples were filtered through 0.45 um aqueous membrane without adding any catalyst but formic acid for 30 min, and the samples were sampled according to a certain time, and the experimental results are shown in Fig. 5, the concentration of Cr(VI) did not change greatly after 20 min of reaction, indicating that the addition of formic acid only had no catalytic effect on Cr(VI). Then a certain amount of MnO_2 was added without formic acid, and there was no big change in the concentration of Cr(VI) within 120 min of the reaction, indicating that only the addition of MnO_2 had no catalytic effect of Cr(VI). Next, a certain amount of Pd/MnO_2 was added without formic acid, and the concentration of Cr(VI) did not change greatly within 120 min, indicating that Cr(VI) could not be reduced or removed by adsorption with the addition of Pd/MnO_2 catalyst only. Finally, when formic acid and catalyst Pd/MnO_2 were added, the Cr(VI) concentration was only 0.068 mM after 120 min of reaction, and the reduction rate reached 93.2%, which shows that the removal of Cr(VI) from this study is essentially a chemical reaction process that requires the joint action of formic acid and a catalyst. The above experimental conditions were kept consistent.

3.2.2. *Influence of different catalysts*

In this paper, the catalytic hydrogenation reduction of Cr(VI) by the Pd/MnO_2 catalyst was studied, and the results are shown in Fig. 6. In heterogeneous catalytic reactions, the transformation of the reactants generally complies with a first-order kinetic model, where the reaction rate decreases gradually as the reaction progresses. By comparing the initial activities of several people, we can see that the reduction reaction rate of the two catalysts is very different. MnO_2 restored only 20.9% of Cr(VI) within 120 min, Pd/MnO_2 restored 93.2% of Cr(VI) within 120 min, and did not fully restore Cr(VI) to Cr(III) within 120 min. Because Pd adsorbs H_2 produced by formic acid on the surface of the metal particles, It dissociates H_2 into H atoms to reduce Cr(VI) to Cr(III). It shows that the loaded precious metal palladium significantly improves the catalytic reaction of format as the hydrogen source system, and it still needs further study.

3.2.3. *Effect of different catalyst dosing amounts*

The study evaluated the effect of the mass transfer resistance during the reaction by changing the amount of the catalyst injection. The results are shown in Fig. 7: the conversion efficiency of the Pd/MnO_2 injection of the catalyst increased significantly, because under the condition of a certain concentration of reactants, raising the amount of catalyst also increases the active site amount of Pd in the reaction liquid, thus effectively promoting the catalytic hydrogenation reduction rate of Cr(VI). However, the initial activity of the catalyst mass calibration has basically changed a

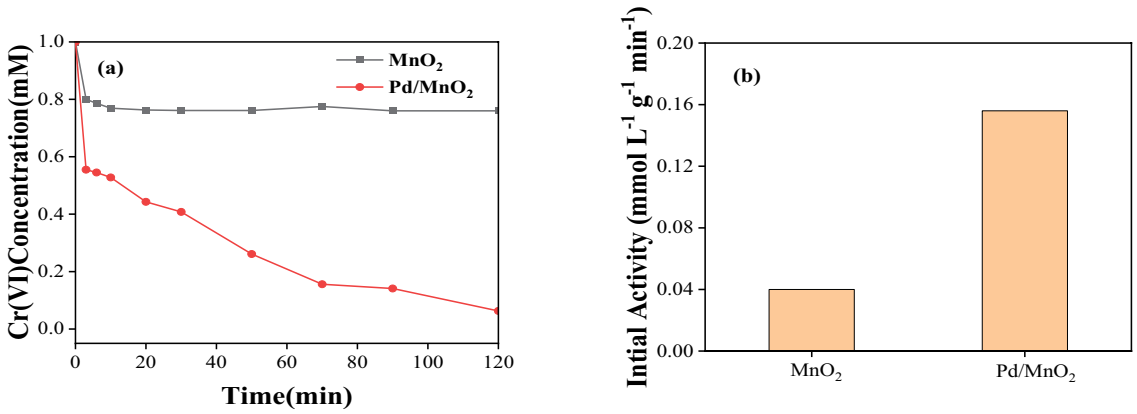

Fig. 6. Catalytic hydrogen reduction reaction of Cr(VI) with different catalysts. Reaction conditions: Cr(VI) concentration is 1.0 mM, hydrogen source is formic acid, pH = 2.0, catalyst dosage is 0.25 g/L. (a) Effect of different catalysts on the hydrogen reduction of Cr(VI) and (b) effect of different catalysts on the initial activity of Cr(VI) hydrogen reduction reaction.

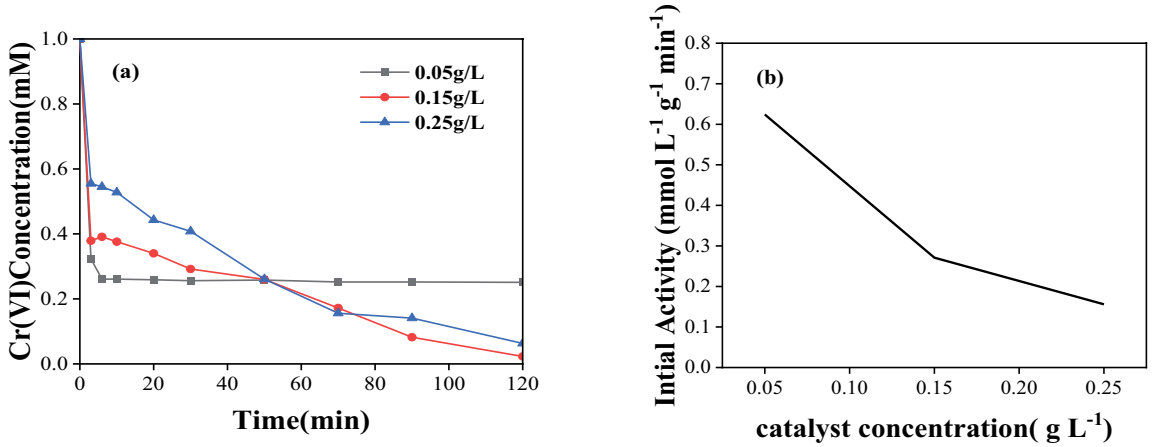

Fig. 7. Catalytic hydrogen reduction reaction of Cr(VI) with different catalyst dosing. Reaction conditions: Cr(VI) concentration is 1.0 mM, hydrogen source is formic acid, pH = 2.0, catalyst is Pd(0.74)/MnO_2. (a) Effect of different Pd/MnO_2 catalyst dosing on the hydrogenation reduction of Cr(VI) and (b) effect of different catalyst dosing on the initial activity of the Cr(VI) hydrogenation reduction reaction.

little, this result shows that the influence of the mass transfer resistance in the reaction is negligible under the present experimental conditions [27].

3.2.4. *Effect of different initial concentrations of Cr(VI)*

By changing the initial concentration of Cr(VI), one can determine the effect of Cr(VI) adsorption on the catalyst carrier on the whole reaction, and the results are shown in Fig. 6. As the initial concentration of Cr(VI) increases, the initial activity of the reaction also gradually increases, indicating that the catalyst adsorption of Cr(VI) strengthens its catalytic hydrogenation and dechlorination reactivity to some extent [28,29]. This result can be fitted with the Langmuir–Hinshelwood model.

$$r_0 = k\theta_s = k\frac{bC_0}{1+bC_0} \quad (1)$$

$$\frac{1}{r_0} = \frac{1}{kbC_0} + \frac{1}{k} \quad (2)$$

where r_0 is the initial activity of hydrogenation reduction when the initial concentration of Cr(VI) is C_0; θ_s is the coverage rate of Cr(VI) adsorbed on the catalyst surface, k is the reaction rate constant, and b is the adsorption equilibrium constant of Cr(VI). Under the same reaction conditions, the higher the initial concentration of Cr(VI) is, the longer the reaction time is required for a complete Cr(VI) reaction. As the initial concentration of Cr(VI) increases, the initial activity of the catalyst reaction also gradually increases, indicating that the reaction rate gradually increases with the initial concentration of Cr(VI). Fig. 8b shows that the $1/r_0$ and $1/C_0$ linear correlation coefficient R^2 is 0.9986, demonstrating that the hydrogenation reduction reaction of Cr(VI) conforms to the Langmuir–Hinshelwood model. It shows that the adsorption process of Cr(VI) on the catalyst surface is the rate control step of the catalytic reduction reaction [30], indicating that Cr(VI) adsorption in the catalyst is the control step of Cr(VI) dechlorination. Promoting the adsorption of Cr(VI) on the surface of the catalyst can facilitate its hydrogenation and dehlorination to some extent.

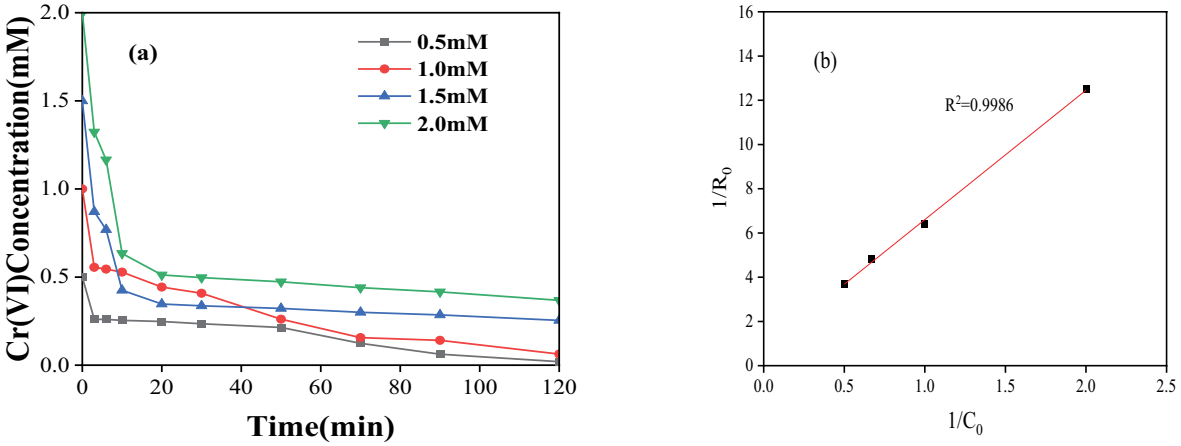

Fig. 8. Different initial concentrations of Cr(VI) on the Cr(VI)-catalyzed hydrogen reduction reaction. Reaction conditions: catalyst is Pd(0.74)/MnO_2, hydrogen source is formic acid, pH = 2.0, catalyst dosage is 0.25 g/L. (a) Effect of different initial concentrations of reactants on the hydrogenation reduction of Cr(VI) and (b) linear relationship between $1/r_0$ and $1/C_0$.

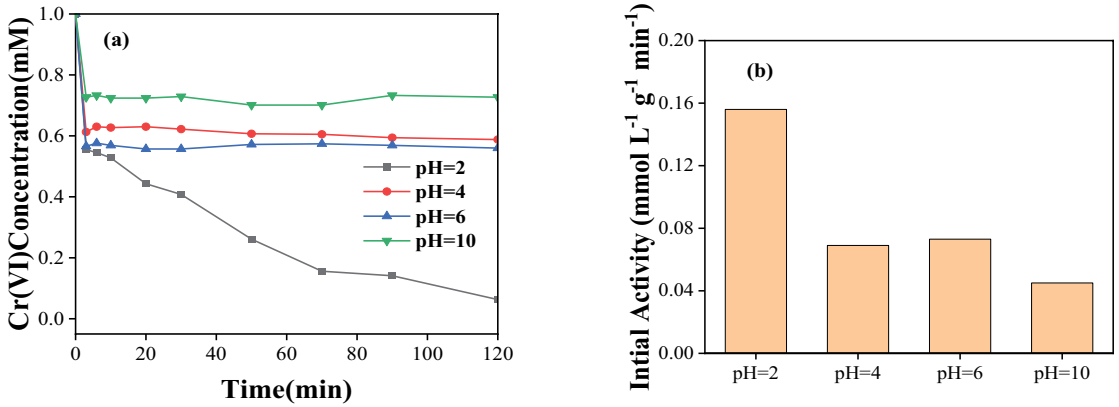

Fig. 9. Different pH on Cr(VI)-catalyzed hydrogen reduction reaction. Reaction conditions: catalyst is Pd(0.74)/MnO_2, Cr(VI) concentration is 1.0 mM, hydrogen source is formic acid, catalyst dosage is 0.25 g/L. (a) Effect of different solution pH on the hydrogenation reduction of Cr(VI) and (b) effect of different solution pH on the initial activity of the hydrogenation reduction reaction of Cr(VI).

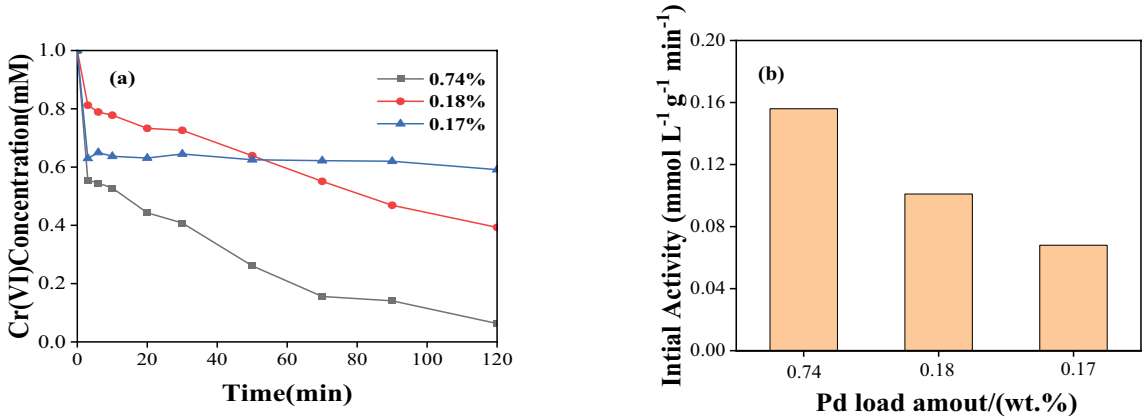

Fig. 10. Catalytic hydrogen reduction reaction of Cr(VI) by loaded Pd/MnO_2 with different Pd loadings. Reaction conditions: Cr(VI) concentration is 1.0 mM, hydrogen source is formic acid, catalyst dosage is 0.25 g/L, pH = 2.0. (a) Effect of different loading on the hydrogen reduction of Cr(VI) and (b) effect of different loading on the initial activity of the Cr(VI) hydrogen reduction reaction.

3.2.5. Effect of different pH

In the catalytic reduction system of Pd/MnO_2 to Cr(VI), solution pH directly affects the surface properties of the catalyst, the ionic form of Cr(VI) and the formation form of the end product. Therefore, the present study explored the catalytic activity of the catalyst for different pH conditions (pH range 2.0–10.0). The results are shown in Fig. 9: When pH rose from 2.0 to 10, the removal efficiency of Cr(VI) decreased from 56.4% to 22.7% within 30 min, that is, high pH inhibited the catalytic conversion of Cr(VI). There are three reasons as follows. First, the increase of pH leads to the deprotonation of the catalyst and reduces the positive charge density on its surface, weakening the electrostatic gravity of Cr(VI) in negative ions on the surface of the catalyst, which reduces the conversion efficiency [31]. Second, the redox potential of Cr(VI) reduced to Cr(III) moves in the positive direction with the pH decrease, indicating that the reduction of Cr(VI) occurs more easily under low pH conditions [32]. Third, in the reaction of pH 4, the later reaction rate is significantly lower than in the initial stage, because the precipitation formed by the reduction product Cr(III) at high pH was deposited on the surface of the catalyst, concealing the active site, thus preventing the further progress of the reaction.

3.2.6. Effect of different Pd loadings

Fig. 10 shows the effect of catalysts with different Pd loads on the hydrogenation reduction rate of Cr(VI). It can be seen that the hydrogenation reduction rate of Cr(VI) is significantly improved with the increase of Pd load. This is because the increase of the Pd load leads to the increase of the Pd active site, which activates the formic acid to obtain the active hydrogen, and the active hydrogen reduces Cr(VI), and finally realizes the reduction of Cr(VI) to the non-toxic Cr(III).

4. Conclusion

In this study, the Pd/MnO_2 catalyst synthesized by impregnation was used for the liquid-phase catalytic hydrogenation reduction of Cr(VI) with good catalytic effect. XRD, TEM, scanning electron microscopy characterization results showed that Pd was successfully dispersed on top of the MnO_2 carrier, which avoided the formation of clusters of Pd and also increased the reaction of the active component Pd with formic acid (hydrogen source), which would produce more active hydrogen, making Cr(VI) easier to become Cr(III) by electron gain. The experimental test results showed that the reduction of Cr(VI) by Pd/MnO_2 was 93.2%, and the reduction of Cr(VI) by MnO_2 was 20.9%, and the reduction of Cr(VI) by MnO_2 after loading Pd was 4.46 times higher than that without Pd. The reduction of Cr(VI) in water was influenced by the acidity of the catalyst surface, which was an adsorption-inhibited reaction; by decreasing the reduction of Cr(VI) in water was influenced by the acidity of the catalyst surface, and the reduction of Cr(VI) could be promoted by reducing the initial concentration of Cr(VI); The high loading of Pd on the Pd/MnO_2 catalyst and the low pH in the solution were both beneficial to the reduction of Cr(VI). The results show that the Pd-loaded MnO_2 catalyst can be used as a highly active catalyst to reduce Cr(VI) in water efficiently and rapidly, which provides a new method for the treatment of Cr(VI) pollution in water.

Ethical approval

There were no studies involving human participants and/or animals in this study.

Consent to participate

All authors agree to participate.

Consent to publish

All authors read and approved the final manuscript.

Author contributions

Yuhong Cao participated in conceptualizing, drafting, collecting and analyzing the experimental data. Dianzhao Li worked on the experiments, drafted the manuscript and revised the manuscript. Daliang Yu and Fan Wen consulted related materials and assisted in the experiments.

Declaration of competing interest

The authors declare that they have no known competing financial interests or personal relationships that could have appeared to influence the work reported in this paper.

Data availability

The datasets generated during and/or analysed during the current study are available from the corresponding authors on reasonable request.

Acknowledgements/funding

The financial support from the National Natural Science Foundation of China (41971175), and Anhui Normal University College Students innovation and Entrepreneurship training program project (2022056511) is gratefully acknowledged.

References

[1] Z. Jiang, X. Huang, Q. Wu, M. Li, Q. Xie, Z. Liu, X. Zou, Adsorption of sulfonamides on polyamide microplastics in an aqueous solution: behavior, structural effects, and its mechanism, Chem. Eng. J., 454 (2023) 140452, doi: 10.1016/j.cej.2022.140452.

[2] R. Xu, Y.-N. Wang, Y. Sun, H. Wang, Y. Gao, S. Li, L. Guo, L. Gao, External sodium acetate improved Cr(VI) stabilization in a Cr-spiked soil during chemical-microbial reduction processes: insights into Cr(VI) reduction performance, microbial community and metabolic functions, Ecotoxicol. Environ. Saf., 251 (2023) 114566, doi: 10.1016/j.ecoenv.2023.114566.

[3] S. Kocaoba, G. Akcin, Removal and recovery of chromium and chromium speciation with MINTEQA$_2$, Talanta, 57 (2002) 23–30.

[4] W. Liu, J. Zheng, X. Ou, X. Liu, Y. Song, C. Tian, W. Rong, Z. Shi, Z. Dang, Z. Lin, Effective extraction of Cr(VI) from hazardous

gypsum sludge via controlling the phase transformation and chromium species, Environ. Sci. Technol., 52 (2018) 13336–13342.
[5] Y. Du, L. Wang, J. Wang, G. Zheng, J. Wu, H. Dai, Flower-, wire-, and sheet-like MnO_2-deposited diatomites: highly efficient absorbents for the removal of Cr(VI), J. Environ. Sci., 29 (2015) 71–81.
[6] X. Tang, J. Wu, W. Wu, Z. Zhang, W. Zhang, Q. Zhang, P. Li, Competitive-type pressure-dependent immunosensor for highly sensitive detection of diacetoxyscirpenol in wheat via monoclonal antibody, Anal. Chem., 92 (2020) 3563–3571.
[7] Z. Zhang, P. Ma, R. Ahmed, J. Wang, D. Akin, F. Soto, U. Demirci, Advanced point-of-care testing technologies for human acute respiratory virus detection, Adv. Mater., 34 (2022) e2103646, doi: 10.1002/adma.202103646.
[8] M. Shi, R. Wang, L. Li, N. Chen, P. Xiao, C. Yan, X. Yan, Redox-active polymer integrated with MXene for ultra-stable and fast aqueous proton storage, Adv. Funct. Mater., 33 (2023) 2209777, doi: 10.1002/adfm.202209777.
[9] Z. Wang, L. Dai, J. Yao, T. Guo, D. Hrynsphan, S. Tatsiana, J. Chen, Enhanced adsorption and reduction performance of nitrate by Fe–Pd–Fe_3O_4 embedded multi-walled carbon nanotubes, Chemosphere, 281 (2021) 130718, doi: 10.1016/j.chemosphere.2021.130718.
[10] Z. Wang, C. Chen, H. Liu, D. Hrynshpan, T. Savitskaya, J. Chen, J. Chen, Enhanced denitrification performance of *Alcaligenes* sp. TB by Pd stimulating to produce membrane adaptation mechanism coupled with nanoscale zero-valent iron, Sci. Total Environ., 708 (2020) 135063, doi: 10.1016/j.scitotenv.2019.135063.
[11] C. Zhao, M. Xi, J. Huo, C. He, L. Fu, Computational design of BC_3N_2 based single atom catalyst for dramatic activation of inert CO_2 and CH_4 gasses into CH_3COOH with ultralow CH_4 dissociation barrier, Chin. Chem. Lett., 34 (2023) 107213, doi: 10.1016/j.cclet.2022.02.018.
[12] M. Xi, C. He, H. Yang, X. Fu, L. Fu, X. Cheng, J. Guo, Predicted a honeycomb metallic BiC and a direct semiconducting Bi_2C monolayer as excellent CO_2 adsorbents, Chin. Chem. Lett., 33 (2022) 2595–2599.
[13] D. Chen, Y. Li, X. Li, X. Hong, X. Fan, T. Savidge, Key difference between transition state stabilization and ground state destabilization: increasing atomic charge densities before or during enzyme–substrate binding, Chem. Sci., 13 (2022) 8193–8202.
[14] M. Li, J. He, Y. Tang, J. Sun, H. Fu, Y. Wan, S. Zheng, Liquid phase catalytic hydrogenation reduction of Cr(VI) using highly stable and active Pd/CNT catalysts coated by N-doped carbon, Chemosphere, 217 (2019) 742–753.
[15] J. Wei, L. Zou, Y. Li, Facile synthesis of hollow structured mesoporous silica nanoreactors with confined ultra-small Pd NPs for efficient hydrogenation reactions, J. Porous Mater., 26 (2019) 157–162.
[16] M.V. Lombardo, M. Videla, A. Calvo, F.G. Requejo, G.J.A.A. Soler-Illia, Aminopropyl-modified mesoporous silica SBA-15 as recovery agents of Cu(II)-sulfate solutions: adsorption efficiency, functional stability and reusability aspects, J. Hazard. Mater., 223 (2012) 53–62.
[17] M. Moritz, M. Łaniecki, SBA-15 mesoporous material modified with APTES as the carrier for 2-(3-benzoylphenyl) propionic acid, Appl. Surf. Sci., 258 (2012) 7523–7529.
[18] L. Mo, W. Yu, H. Cai, H. Lou, X. Zheng, Hydrodeoxygenation of bio-derived phenol to cyclohexane fuel catalyzed by bifunctional mesoporous organic–inorganic hybrids, Front. Chem., 6 (2018) 216, doi: 10.3389/fchem.2018.00216.
[19] A. Al-Nayili, H.S. Majdi, T.M. Albayati, N.M.C. Saady, Formic acid dehydrogenation using noble-metal nanoheterogeneous catalysts: towards sustainable hydrogen-based energy, Catalysts, 12 (2022) 324, doi: 10.3390/catal12030324.
[20] Y. Yuan, C. Liu, B.W. Byles, W. Yao, B. Song, M. Cheng, J. Lu, Ordering heterogeneity of [MnO_6] octahedra in tunnel-structured MnO_2 and its influence on ion storage, Joule, 3 (2019) 471–484.
[21] S.K. Ghosh, Diversity in the family of manganese oxides at the nanoscale: from fundamentals to applications, ACS Omega, 5 (2020) 25493–25504.
[22] S. Dai, N. Wang, C. Qi, X. Wang, Y. Ma, L. Yang, X. Wang, Preparation of core-shell structure Fe_3O_4@C@MnO_2 nanoparticles for efficient elimination of U(VI) and Eu(III) ions, Sci. Total Environ., 685 (2019) 986–996.
[23] M. Dubey, N.V. Challagulla, S. Wadhwa, R. Kumar, Ultrasound assisted synthesis of magnetic Fe_3O_4/α-MnO_2 nanocomposite for photodegradation of organic dye, Colloids Surf., A, 609 (2021) 125720, doi: 10.1016/j.colsurfa.2020.125720.
[24] H. Lv, Y. Yuan, Q. Xu, H. Liu, Y.G. Wang, Y. Xia, Carbon quantum dots anchoring MnO_2/graphene aerogel exhibits excellent performance as electrode materials for supercapacitor, J. Power Sources, 398 (2018) 167–174.
[25] C. Lang, Y. Jia, X. Yao, Recent advances in liquid-phase chemical hydrogen storage, Energy Storage Mater., 26 (2020) 290–312.
[26] J. Zheng, H. Zhou, C.G. Wang, E. Ye, J.W. Xu, X.J. Loh, Z. Li, Current research progress and perspectives on liquid hydrogen rich molecules in sustainable hydrogen storage, Energy Storage Mater., 35 (2021) 695–722.
[27] B. Singh, J. Na, M. Konarova, T. Wakihara, Y. Yamauchi, C. Salomon, M.B. Gawande, Functional mesoporous silica nanomaterials for catalysis and environmental applications, Bull. Chem. Soc. Jpn., 93 (2020) 1459–1496.
[28] M. Turáková, T. Salmi, K. Eränen, J. Wärnå, D.Y. Murzin, M. Králik, Liquid phase hydrogenation of nitrobenzene, Appl. Catal., A, 499 (2015) 66–76.
[29] C. Fernandez-Ruiz, S. Liu, J. Bedia, J.J. Rodriguez, L.M. Gómez-Sainero, Enhanced selectivity to olefins in the hydrodechlorination of trichloromethane using Ag-Pd on activated carbon catalysts, J. Environ. Chem. Eng., 9 (2021) 104744, doi: 10.1016/j.jece.2020.104744.
[30] P. Zou, Z.H. Ren, P.F. Zhu, R.M. Xie, Y.X. Gou, Q. Zhang, Preparation and performance study of Ce-$BiVO_4$/Fe_3O, Mod. Chem. Ind., 39 (2019) 83–87.
[31] O. Fizer, M. Fizer, V. Sidey, Y. Studenyak, Predicting the end point potential break values: a case of potentiometric titration of lipophilic anions with cetylpyridinium chloride, Microchem. J., 160 (2021) 105758, doi: 10.1016/j.microc.2020.105758.
[32] M. Liao, X. Wang, S. Cao, M. Li, X. Peng, L. Zhang, Oxalate modification dramatically promoted Cr(VI) removal with zero-valent iron, ACS EST Water, 1 (2021) 2109–2118.